Photooxidation of Organic Sulfide Enhanced by Heavy Atom Effect in Porphyrin Metal-Organic Frameworks with a Sea Topology

Matthew J. Tang,[a,†] Juan C. Arriaga Gomez,[a,†] Doroteo Manriquez,[a,†] Dr. Xiyuan Yao,[a] Dr. Yajiao Hao,[a] Dr. Haoyuan Chen,[b] Dr. Yuting Li,[c] Dr. Lun An,[c] Dr. Long Qi,[c] Dr. Omar K. Farha,[d] Dr. Matthias Selke,[a,*] and Dr. Yangyang Liu[a,*]

[a] Department of Chemistry and Biochemistry, California State University, Los Angeles, 5151 State University Drive, Los Angeles, CA 90032, United States

[b] Department of Chemistry, Southern Methodist University, 3215 Daniel Ave., Dallas, Texas 75275, United States

[c] U.S. DOE Ames National Laboratory, Iowa State University, 2416 Pammel Dr., Ames, Iowa 50011, United Stated

[d] Department of Chemistry and International Institute for Nanotechnology (IIN), Northwestern University, Evanston, Illinois 60208, United States; Department of Chemical and Biological Engineering and Paula M. Trienens Institute for Sustainability and Energy, Northwestern University, Evanston, Illinois 60208, United States

*Corresponding authors: yliu114@calstatela.edu (Y.L.); mselke@calstatela.edu (M.S.)

† These authors contributed equally to this work

KEYWORDS

Metal-organic frameworks, photooxidation, sulfur mustard, singlet oxygen, textiles, heavy atom effect

ABSTRACT

The photoactivity of three porphyrin-based metal-organic frameworks (PMOFs) incorporating Al, Ga, and In nodes was systematically evaluated using the photooxidation of an organic sulfide (2-chloroethyl ethyl sulfide, or CEES; a mustard gas simulant). Faster photodegradation of CEES was observed for PMOFs with heavier metal nodes, placing In-PMOF as the most efficient photocatalyst in the series. Guided by this insight, we developed CSLA-10, a MOF integrating In nodes and Sn-doped porphyrin linker to synergistically amplify heavy-atom effects at both the nodes and ligand levels. CSLA-10 exhibited the fastest reported CEES photooxidation to date, achieving a half-life of 38 s in methanol under blue LED irradiation. When grafted onto textiles, CSLA-10 enabled solvent-free CEES degradation in air/O_2 with a half-life of 2.7 min and complete conversion within 7 min, representing the most rapid full degradation reported under solvent-free conditions. This work establishes a dual heavy-atom strategy for enhancing intersystem crossing and singlet oxygen generation in porphyrin MOFs, providing a rational design principle for next-generation photocatalysts for the degradation of toxic organic sulfides.

Introduction

Reactive oxygen species (ROS), such as singlet oxygen ($^1O_2$), hydrogen peroxide (H_2O_2), superoxide ($\bullet O_2^-$), and hydroxyl radical (•OH), are highly reactive species derived from molecular oxygen (O_2). In photocatalytic systems, ROS are essential intermediates for the synthesis of value-added products and the photodegradation of organic pollutants.[1-3] Conventional thermal catalytic processes often require elevated temperatures and pressures, as well as sacrificial chemical oxidants. In contrast, photochemically driven processes can typically proceed under ambient conditions, offering a more sustainable alternative. The mild operating conditions of photoinduced oxidation also enable improved product selectivity and enhanced catalyst reusability.[4-5] For example, energy-efficient photochemical methods have been developed for the selective oxidation of hydrocarbons, alcohols, and organic sulfides.[1, 6-7] In addition, advanced oxidation processes that rely on ROS have been widely employed for the degradation of organic contaminants, including phenols and dyes, under visible or ultraviolet (UV) irradiation.[2, 8]

ROS can be generated through the photosensitization of various photoactive compounds and materials under light irradiation. Among these, metal-organic frameworks (MOFs), renowned for their permanent porosity and well-defined crystalline structures, have been extensively investigated as platforms for ROS generation and have demonstrated strong performance across a wide range of photocatalytic applications.[9-10] The three-dimensional (3-D) architectures of MOFs spatially organize photosensitizers into ordered arrays, which helps suppress aggregation and mitigate photodegradation. Their high surface areas enable the enrichment of O_2 and substrates within the pores, facilitating their conversation into ROS and reactive intermediates. Moreover, the intrinsic porosity of MOFs promotes efficient diffusion of ROS and substrates throughout the frameworks. Collectively, these structural features endow MOFs with enhanced photoactivity and

catalytic efficiency. Importantly, the modular and tunable nature of MOFs allows for the rational design of photosensitizing materials through diverse combination of metal nodes and organic linkers.

Porphyrin-based MOFs (PMOFs), constructed from organic linkers bearing functional porphyrin centers, represent a class of highly effective photoactive materials for ROS generation and have demonstrated significant potential in photocatalysis, photodynamic therapy, and environmental remediation.[11-13] For example, Zr-based PMOFs such as Zr-PCN-222/MOF-545 exhibit high activity for the selective photodegradation of 2-chloroethyl ethyl sulfide (CEES), a mustard gas simulant, to its less toxic product 2-chloroethyl ethyl sulfoxide (CEESO) (**Figure 1a**).[14] Mechanistic studies have shown that $^1O_2$ is the primary ROS responsible for CEES oxidation in these Zr-PMOFs.[14-15] Our group recently investigated the structure-property relationship for Zr-PMOFs with varying topologies, metal node connectivities, and pore sizes/shapes. We found that higher surface areas correlate with faster oxidation of CEES to CEESO in methanol, primarily due to enhanced diffusion of reactants and products within the framework.[15] Additionally, we demonstrated that sulfoxide selectivity is mainly dependent on the solvent – protic solvents (e.g., methanol) afford higher selectivity toward CEESO (the less toxic product) than aprotic solvents (e.g., acetonitrile). In contrast, variations in metal node connectivity and overall framework topology were found to have minimal influence on the reaction rate and selectivity.[15]

To date, most PMOFs investigated for the degradation of organic sulfides have been Zr-based, containing Zr_6 oxo clusters and porphyrin linkers, such as PCN-222/MOF-545, MOF-525, and PCN-223.[14-15] Although previous studies revealed that the connectivity of Zr_6 node has minimal influence on the photoactivity of Zr-PMOFs,[15] the impact of other metal nodes containing different metal ions on photocatalytic performance of PMOFs remains largely unexplored. The heavy atom

effect is a well-established phenomenon observed in photosensitizers, including porphyrins, in which heavier atoms enhance spin-orbital coupling (SOC) and promote intersystem crossing (ISC), thereby increasing ROS generation efficiency.[16-18] For example, PMOFs incorporating metalated porphyrin centers, particularly those containing heavy metal centers such as In or Sn, demonstrated enhanced activity toward sulfide oxidation.[19] In addition, Howarth and coworkers recently reported accelerated CEES oxidation in MOFs featuring heavier rare-earth metal nodes and a tetratopic pyrene linker.[20-21] Despite these findings, it remains unclear whether incorporating heavy metal nodes into PMOFs can directly facilitate ROS generation and thereby accelerate the photooxidation of organic sulfides.

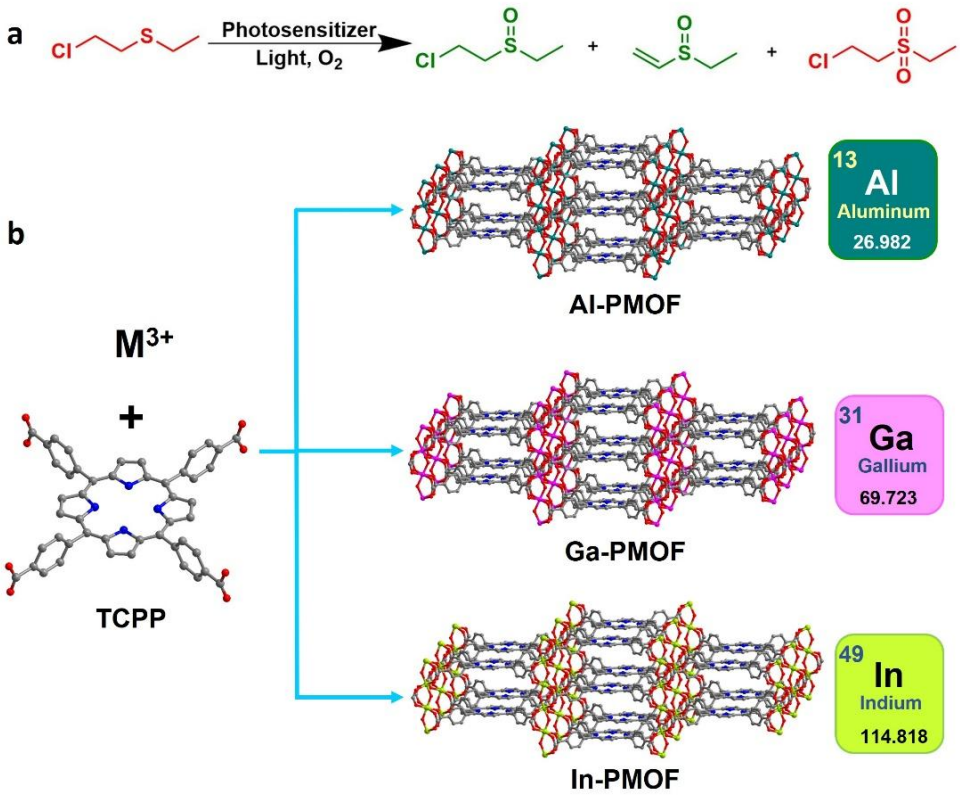

Figure 1. (a) Photooxidation of 2-chloroethyl ethyl sulfide (CEES), a mustard gas simulant, to the less toxic oxidation products 2-chloroethyl ethyl sulfoxide (CEESO) and ethyl vinyl sulfoxide (EVSO), as well as the toxic product 2-chloroethyl ethyl sulfone ($CEESO_2$) in the presence of

photosensitizers and O_2. (b) Crystal structures of three PMOFs constructed from Al-, Ga-, and In-oxo one-dimensional (1-D) chains and tetrakis(4-carboxyphenyl)porphyrin (TCPP) linkers.

This work aims to elucidate the role of metal nodes in governing the photoactivity of PMOFs. We investigated the photodegradation of an organic sulfide (CEES) using PMOFs constructed from tetrakis(4-carboxyphenyl)porphyrin (TCPP) linker and different metal nodes (M = Al, Ga, and In), namely Al-PMOF,[22] Ga-PMOF,[23] and In-PMOF[23] (structures shown in **Figure 1**b). Their efficiency of $^1O_2$ generation was probed using CEES photooxidation under blue LED irradiation. We observed that PMOFs incorporating heavier metal nodes exhibited progressively faster CEES degradation, with In-PMOF emerging as the most active catalyst in the series, achieving a half-life ($t_{1/2}$) of 1.4 min in MeOH. To further amplify the heavy atom effect, the TCPP linker was doped with Sn and incorporated into the In-PMOF framework. As predicted, the resulting In-PMOF(Sn) (CSLA-10) displayed a markedly enhanced photooxidation rate, achieving an exceptionally short half-life of 38 s in MeOH under blue LED irradiation. Furthermore, textiles grafted with CSLA-10 with benzoic acid additives exhibited a half-life of 2.7 min under blue LEDs in air under solvent-free conditions, reaching > 99% CEES photooxidation within 7 min. To our knowledge, CSLA-10 represents the fastest reported photocatalyst for CEES degradation in both solution and solvent-free systems. This work demonstrates that incorporating heavier elements into both the metal nodes and porphyrin ligands of photoactive MOFs is an effective strategy for enhancing photocatalytic performance.

Experimental Section

Materials and Instrumentation. 2-chloroethyl ethyl sulfide (CEES, 98%), and deuterated chloroform ($CDCl_3$, 99.5%) were purchased from Across Organics. Benzoic acid (BA, 99.5%), acetic acid (80%), methanol (MeOH, 99.8%), acetonitrile (MeCN, 99.9%), dichloromethane (DCM, 99.5%), *N, N*-dimethylformamide (DMF, 99.9%), aluminum trichloride hexahydrate ($AlCl_3 \cdot 6H_2O$, 99.9%), indium (III) nitrate trihydrate ($In(NO_3)_3 \cdot H_2O$, 99.9%), hydrogen peroxide (H_2O_2, 30%), ammonium molybdate (IV) tetrahydrate (99+%), sodium hydroxide (98%), 1-bromo-3,5-difluorobenzene (98%), and potassium iodide (99.99%) were purchased from Fisher Scientific. Potassium hydrogen phthalate (99.8%), 5,5-dimethyl-1-pyrroline *N*-oxide (DMPO, 97%), and 1,4-diazabicyclo[2.2.2]octane (DABCO, >98%) were purchased from TCI America. *meso*-Tetra(4-carboxyphenyl)porphyrin (TCPP, 97%) was obtained from Frontier Scientific. Gallium(III) nitrate hydrate (99.9%) and 9,10-dimethylanthracene (DMA, 99%) were purchased from Sigma Aldrich. 2,2,6,6-Tetramethylpiperidine (TEMP, 98%) was obtained from Alfa Aesar. All reagents were used as received without further purification. Instrumentation details are provided in the Supporting Information (SI).

Synthesis of PMOFs. The syntheses of Al-PMOF, Ga-PMOF, and In-PMOF were adapted from literature,[22-23] with detailed procedures described in the SI. CSLA-10 was synthesized by dissolving TCPP(Sn) (51.6 mg) in DMF (2.17 mL) to in a 35 mL glass pressure vessel, followed by sonication for 20 min. Subsequently, 0.23 mL of 0.5 M $In(NO_3)_3$ solution was added, and the mixture was sonicated for an additional 20 min. The reaction mixture was then heated at 120 ºC for 48 h and allowed to cool to room temperature over 6 hours. The resulting purple crystals were collected and washed with DMF (3 × 10 mL) and acetone (3 × 10 mL). The product were dried in a vacuum oven at 90 ºC for 18 h and subsequently activated under vacuum at 140 ºC for 16 h.

Preparation of MOF/Additive/Textile Composites. The textile composites were prepared following the procedures reported by Hao et al.[15] Al-PMOF (14.0 mg; alternatively, 15.3 mg Ga-PMOF, 16.6 mg In-PMOF, or 18.5 mg CSLA-10) and benzoic acid (144.0 mg) were dispersed in 1 mL of acetone and sonicated for 20 min to afford a homogeneous suspension. A 2 cm × 2 cm cotton textile was immersed in the suspension and dried in an oven at 60 ºC for 5 min. The textile was then re-immersed in the suspension and dried again. This dip-dry cycle was repeated until the entire suspension was consumed, ensuring complete deposition of the MOF and additives onto the cotton substrate. The resulting textile composite was further dried in an oven at 60 ºC for 18 h and subsequently cut into four 1 cm × 1 cm pieces for further testing.

Photocatalytic Studies and Reusability Tests. The photooxidation experiments conducted in organic solvents and under solvent-free conditions followed procedures previously reported by Hao et al.,[15] with detailed experimental protocols described in the SI. For the reusability studies, five consecutive catalytic cycles were performed under the same conditions as the solvent-free photooxidation experiments, using a balloon filled with air and a solar simulator as the light source. Each reaction was allowed to proceed for 1 h to ensure complete CEES conversion. Product selectivity was determined by extracting the reaction mixture with $CDCl_3$, followed by ^1H NMR analysis.

Singlet Oxygen Trapping Experiments. Under dark (aphotic) conditions, a stock solution of DMA was prepared by dissolving 4.0 mg DMA in 8 mL of MeCN with sonication for 10 min. The solution was subsequently diluted by 50% twice to obtain an absorbance of approximately 1. In a quartz tube, 3.70 mg of Al-PMOF (4.03 mg Ga-PMOF, 4.39 mg In-PMOF, or 5.00 mg CSLA-10; each MOF contains an equivalent amount of porphyrin centers) was dispersed in 6 mL of the diluated DMA stock solution. The suspension was purged with O_2 for 1 min and centrifuged for 5

min. At t = 0, an aliquot (3 mL) was withdrawn, passed through a syringe filter, and analyzed by UV-Vis spectrometry. The analyzed solution was then returned to the quartz tube. The suspension was irradiated by a halogen lamp set to 12.00 amps, equipped with a long-pass cutoff filter that transmits above 493 nm, while being continuously purged with a slow stream of O_2. Aliquots were collected and analyzed at irradiation times of 5, 10, 15, and 20 min. For In-PMOF, aliquots were collected at shorter intervals (0, 1, 1.5, 2, and 2.5 min) due to its faster reaction rate.

Singlet Oxygen Inhibition Experiments. To determine whether $^1O_2$ is the primary oxidant responsible for the oxidation of CEES, inhibition experiments were conducted using a $^1O_2$ quencher, 1,4-diazabicyclo[2.2.2]octane (DABCO). 1.1 mg of Al-PMOF (1.22 mg Ga-PMOF, 1.30 mg In-PMOF, or 1.51 mg CSLA-10) was dispersed in 2 mL MeOH or MeCN in a sealed quartz tube and sonicated for 20 min. The suspension was then purged with O_2 for 20 min. 23 μL of CEES (0.2 mmol, 100 mM) and 5 μL of internal standard (1-bromo-3,5-difluorobenzene, 0.04 mmol) were added to the sealed quartz tube with a microsyringe. At t = 0, a 50 μL aliquot was withdrawn, passed through a syringe filter into a GC autosampler vial, and diluted to 0.5 mL for GC-MS analysis. The reaction mixture was subsequently irradiated with red LEDs, and samples were collected every 20 s for 3 min. The experiments were repeated in 2 mL of 0.25 mM DABCO (0.0005 mmol), 2.5 mM DABCO (0.005 mmol), 25 mM DABCO (0.05 mmol), or 1 M DABCO (2 mmol) solutions in MeOH or MeCN to evaluate the inhibitory effect of DABCO on CEES photooxidation.

Hydrogen Peroxide Trapping Experiments. 1.1 mg Al-PMOF (1.22 mg Ga-PMOF, 1.30 mg In-PMOF, or 1.51 mg In-PMOF(Sn)) was dispersed in 1 mL of MeOH and sonicated for 20 min. The suspension was purged with O_2 for 20 min, followed by 20 min of irradiation under blue LEDs. After irradiation, 2 mL of a detection solution containing potassium iodide (33 g L^{-1}), sodium

hydroxide (1 g L^{-1}), ammonium molybdate tetrahydrate (0.1 g L^{-1}), and potassium hydrogen phthalate (10 g L^{-1}) was added to the MOF suspension. After gentle swirling, 1 mL aliquot was diluted to 5 mL with MeOH, and the production of H_2O_2 was quantified by recording the UV-Vis absorption at 350 nm. The H_2O_2 concentration was determined using linear regression analysis based on a calibration curve constructed from standard solutions of H_2O_2 in MeOH at five concentrations: 0.1 mM, 0.5 mM, and 1.0 mM. 0.125 mM, and 0.0625 mM.

Electron Paramagnetic Resonance (EPR) Spin-Trapping Experiments. In-PMOF (2.64 mg) or In-PMOF(Sn) (3.02 mg) was suspended in 1 mL of dry MeCN and sonicated for 20 min to obain a homogeneous suspension. An aliquot of the MOF suspension (0.4 mL) was mixed with 0.4 mL of TEMP or DMPO solution (0.2 M in dry MeCN) in a quartz tube. The mixture was purged with O_2 for 5 min before being irradiated with blue LEDs for 10 min. Following irradiation, the suspension was passed through a syringe filter to remove the MOF particles, and a 40 μL aliquot of the filtrate was immediately transferred to an EPR flat cell for EPR analysis.

Results and Discussion

Photoactivity of M-PMOFs. Three M-PMOFs incorporating different metal nodes (M = Al, Ga, and In) were synthesized and activated following procedures adapted from previous literature (see SI for details).[22-23] The three MOFs crystallize in the same space group (*Cmmm*) and exhibit similar unit cell parameters (**Table S1**). As shown in **Figure 1b and Figure S1**, all three PMOFs are constructed from one-dimensional (1-D) metal-oxo chains, in which adjacent metal ions are bridged by μ_2-OH groups. The TCPP ligands are arranged in alternating layers interconnected by these 1-D metal chains, forming a characteristic **sea** topology (**Figure S2**). The structure and phase purity of the three PMOFs were confirmed using powder X-ray diffraction (PXRD) (**Figure S3a-**

c). Nitrogen adsorption-desorption isotherms were measured at 77 K to determine the Brunauer-Emmett-Teller (BET) surface areas, which are consistent with previously reported values (**Figure S3d**, **Table 1**). Thermogravimetric analysis revealed similar thermal decomposition profiles for all three PMOFs, with rapid weight loss occurring at approximately 350 °C (**Figure S3e**). Scanning electron microscope (SEM) images showed sheet-like morphologies for all three MOFs, in agreement with their layered crystal topology (**Figure S4**).

Table 1. Surface areas of M-PMOFs and the half-lives and sulfoxide selectivities for CEES photooxidation in O_2 under blue LED irradiation.[i]

MOFs	Surface area (m^2/g)	Half-life ($t_{1/2}$, min)	Sulfoxide selectivity (%)[ii]
Al-PMOF	1,197	4.9	99
Ga-PMOF	1,351	1.8	96
In-PMOF	1,294	1.4	96

[i] All CEES photooxidation reactions were performed with a 0.5 mol% catalyst loading (calculated based on porphyrin centers). At least three catalytic runs were conducted to ensure reproducibility. Reported half-lives and selectivity values represent the average of three independent experiments.

[ii] Two less toxic sulfoxide products were observed: 2-chloroethyl ethyl sulfoxide (CEESO) and ethyl vinyl sulfoxide (EVSO)

After confirming the structures and permanent porosity of the three PMOFs, we assessed their photocatalytic performance for CEES degradation in methanol (MeOH). At a porphyrin loading of 0.5 mol%, all three PMOFs exhibited rapid CEES oxidation in O_2-saturated MeOH under blue LED irradiation, with half-lives ranging from 4.9 to 1.4 min (**Table 1**; **Figure S5a**). Among the series, In-PMOF exhibited the highest activity, achieving a half-life of 1.4 min despite having a

slightly lower surface area than Ga-PMOF. Complete CEES conversion was reached within 3 min in the presence of In-PMOF. In contrast, Al-PMOF showed the slowest degradation rate ($t_{1/2}$ = 4.9 min, while Ga-PMOF displayed intermediate activity ($t_{1/2}$= 1.8 min). In MeOH, all three PMOFs demonstrated high selectivity toward sulfoxide formation, affording 96-99% selectivity for CEES oxidation (**Table 1**).

We then evaluated the photocatalytic performance of the PMOFs on textiles under solvent-free conditions to demonstrate their practical applicability. Following a method reported in one of our previous studies,[15] PMOFs were incorporated into textiles using a dip-coating method (see Experimental Section). In our earlier study, we showed that the addition of benzoic acid (BA) additives to MOF textiles accelerated CEES degradation and enhanced sulfoxide selectivity due to its hydrogen bond donor properties.[15] Using a similar procedure, PMOFs were co-deposited with BA onto textiles, as illustrated in **Figure 2a**. The resulting MOF textiles were characterized using PXRD to confirm the presence of the PMOFs and benzoic acid (**Figure 2b** and **Figure S6**). Their photocatalytic activity toward CEES degradation was assessed by irradiating the CEES-loaded textiles under blue LEDs in an O_2 atmosphere. All reactions were conducted using a 3 mol% MOF loading, calculated based on porphyrin centers. Reaction conversions at various time points and final oxidation products were analyzed using gas chromatography coupled with mass spectrometry (GC-MS) and nuclear magnetic resonance (NMR) spectroscopy. The CEES photooxidation experiments on each textile were performed at least in triplicate to ensure reproducibility (**Figure S5**).

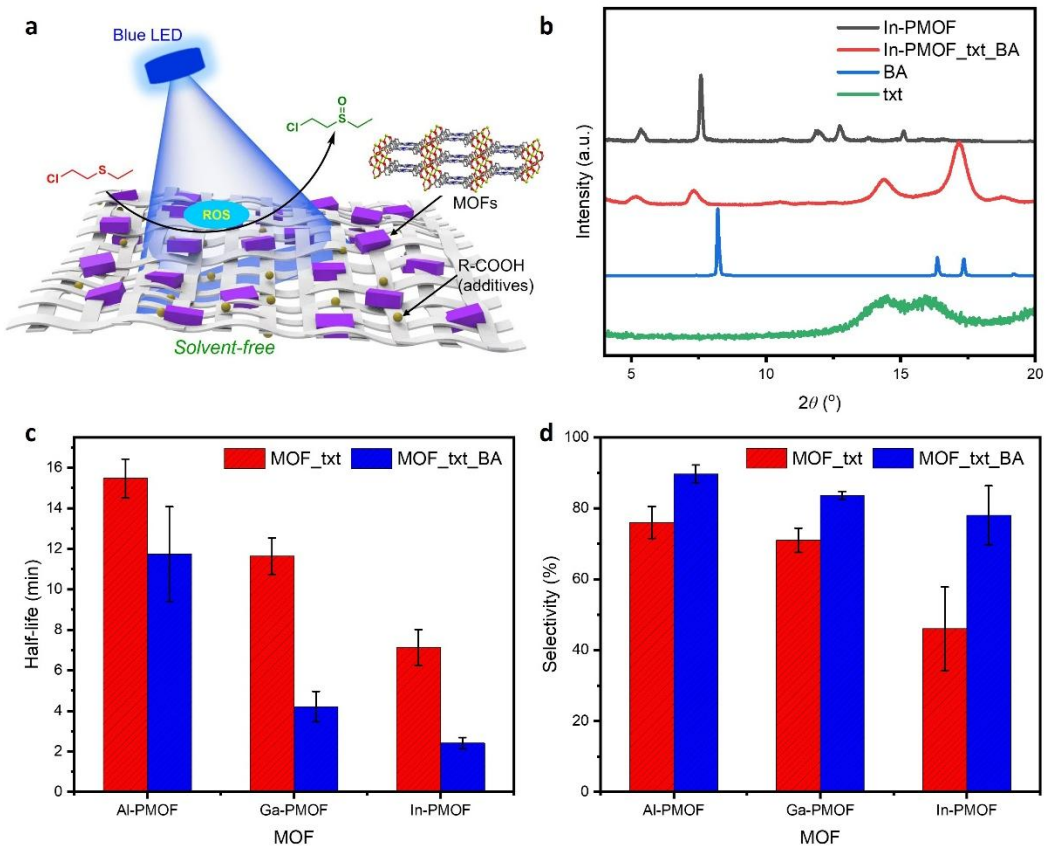

Figure 2. (a) Schematic illustration of MOF textiles incorporating benzoic acid (BA) additives for solvent-free CEES degradation under blue LED irradiation. (b) PXRD patterns of In-PMOF, In-PMOF textile with BA additive, pure BA, and blank textile. (c) Comparison of the half-lives and (d) selectivities for CEES photooxidation on various M-PMOF textiles (M = Al, Ga, In) without additives (MOF_txt) and with benzoic acid (MOF_txt_BA).

The photocatalytic performance of the various textiles for CEES degradation is summarized in **Figure 2cd** and **Figure S5**. Both MOF textiles, with and without BA additives, followed the same activity trend observed for PMOF powders in MeOH (CEES degradation rate: In-PMOF > Ga-PMOF > Al-PMOF), as shown in **Figure 2c** and **Figure S5**. Among them, the textile incorporating In-PMOF with BA additives showed the fastest CEES degradation under blue LED irradiation in an O_2 atmosphere, achieving a half-life of 2.4 min and complete conversion within

10 min. Notably, this is the shortest reported half-life for CEES degradation among MOF-based composites under solvent-free conditions (**Table S2**).[15, 24-27] The retention of high catalytic efficiency under solvent-free conditions highlights the practical potential of these materials for applications in protective masks and clothing. Furthermore, the MOF textiles containing BA additives generally exhibited higher sulfoxide selectivity than those without additives (**Figure 2**d), consistent with our previous findings that hydrogen bond donors such as BA promote sulfoxide formation over sulfone production.[15] Overall, the best-performing material among the three PMOF textiles was the In-PMOF textile with benzoic acid as an additive, which achieved a CEES degradation half-life of 2.4 min and a sulfoxide selectivity of 78% (**Table S3**).

Reactive oxygen species and heavy atom effect. Given that the three PMOFs share the same **sea** topology and possess comparable surface areas, the observed differences in photocatalytic efficiency likely arise from variations in their metal nodes. The presence of heavier In^{3+} ions in the In-PMOFs may enhance ROS generation, thereby leading to faster CEES photooxidation. To confirm this hypothesis, we first investigated the types of ROS produced by the PMOFs. The generation of $^1O_2$ by the PMOFs was probed using 9,10-dimethylanthracene (DMA), a singlet oxygen-specific trap that undergoes a [4+2] cycloaddition to form an endoperoxide (**Figure S7**).[28] Since DMA is also photosensitive, a long-pass filter that transmits above 493 nm was employed so that the DMA was not excited. In all cases, we observed rapid formation of the DMA endoperoxide, confirming $^1O_2$ as the primary oxidant (**Figure S7-8**). In addition, time-resolved $^1O_2$ trapping experiments using DMA revealed the fastest $^1O_2$ generation by In-PMOF (**Figure S7**), consistent with its superior performance in CEES degradation. These results support our hypothesis that incorporation of heavier metal ions, such as In^{3+}, into PMOFs enhances ROS generation, particularly $^1O_2$, thereby improving their photocatalytic activity.

In addition to singlet oxygen, porphyrin-based MOFs may generate hydrogen peroxide (H_2O_2) upon irradiation,[19] and H_2O_2 is known to rapidly oxidize sulfides to sulfoxides.[29-30] To evaluate whether H_2O_2 could act as an active oxidant during our photooxidation protocol, suspensions of the various PMOFs (Al-PMOF, Ga-PMOF, and In-PMOF) in MeOH were irradiated with blue LEDs for 20 min under conditions identical to those used for CEES photooxidation experiments, but in the absence of CEES. Subsequent iodometric titrations using KI detected only trace amounts of H_2O_2. The measured H_2O_2 concentrations were less than 0.5 % of the CEES concentrations employed in the CEES oxidation experiments (**Figure S9** and **Table S4**). The results indicate that H_2O_2 does not play a significant role as an oxidant in the CEES photooxidation process.

Although EPR spin-trapping experiments confirmed the formation of $^1O_2$ and radical species during irradiation (**Figure S10**), the detection of a given ROS does not necessarily establish its direct involvement in the photooxidation process.[31] To quantify the contribution of $^1O_2$ to CEES oxidation, inhibition experiments were performed by adding a singlet oxygen-specific quencher, 1,4-diazabicyclo[2.2.2]octane (DABCO), to the photooxidation reaction mixture. Computational studies indicate that both CEES and DABCO can enter the MOF pores (**Figures S11-S12**), supporting the suitability of DABCO for quenching experiments in these systems. The addition of 25 mol% DABCO (25 mM relative to 100 mM CEES) resulted in a dramatic slowdown of the reaction, with only 23% conversion after 5 min of irradiation, whereas complete conversion was achieved in the absence of DABCO over the same time period (**Figure S13**). The Foote β-value for DABCO in MeOH is 6.5 x 10^{-3} M,[32] where $\beta = k_d/k_q$ (k_d is the rate constant for singlet oxygen deactivation in neat MeOH, and k_q is the quenching rate constant by DABCO). Assuming a value of k_d for singlet oxygen in MeOH of *ca*. 10^4 s^{-1}, we, therefore, estimate the rate constant for singlet oxygen quenching by DABCO (k_q) in MeOH to be 1.5 x 10^7 $M^{-1}s^{-1}$. The rate constant for the

interaction of singlet oxygen with CEES in MeOH has not been reported, but an upper limit for this value would be the rate constant of the interaction of diethyl sulfide with singlet oxygen in MeOH, which has been measured to be 1.7 x 10^7 $M^{-1}s^{-1}$.[33] This value is very similar to the value for DABCO. Thus, a considerable excess of DABCO would be required to fully suppress CEES oxidation if singlet oxygen were the sole oxidant. We therefore conducted additional experiments with a 10-fold excess of DABCO (1 M relative to 100 mM CEES) in MeOH, and complete inhibition of sulfide oxidation was observed for all PMOFs under these conditions. Since MeOH may suppress the formation of free radicals, the quenching experiments were repeated in acetonitrile. In aprotic solvents, DABCO is a considerably more efficient singlet oxygen quencher (k_q = 5.5 x 10^8 $M^{-1}sec^{-1}$),[34] and complete inhibition of product formation was again observed when a 10-fold excess of DABCO was used (**Figure S13**). Collectively, these results demonstrate that $^1O_2$ is the primary ROS responsible for CEES oxidation with minimal, if any, contribution from radical species or hydrogen peroxide.

The effect of added acid (benzoic acid) in our solid-state experiments further supports singlet oxygen as the primary oxidant. Bonesi et al. reported that added acid (<< 0.1% for phenols and carboxylic acids) significantly increases the efficiency of photooxidation of organic sulfides in aprotic media.[35] Consistent with this observation, textiles incorporating benzoic acid showed faster CEES photooxidation than their additive-free counterparts for all three PMOFs (**Figure 2c, Figure S5**).

Rational design of a new MOF. Inspired by the heavy atom effect observed in the M-PMOFs, we introduced an additional heavy atom, Sn, into the TCPP linker to construct an In-based PMOF incorporating Sn-metalated TCPP. The resulting new MOF, In-PMOF(Sn) or (as we named it) CSLA-10, is expected to be isostructural to the free-base In-PMOF but with Sn-TCPP serving as

the organic linker (**Figure 3a**). We hypothesized that the combination of the relatively heavy In^{3+} ions in the metal nodes and the heavy Sn^{4+} centers in the porphyrin ligands could work synergistically to further enhance intersystem crossing and accelerate the photooxidation of CEES.

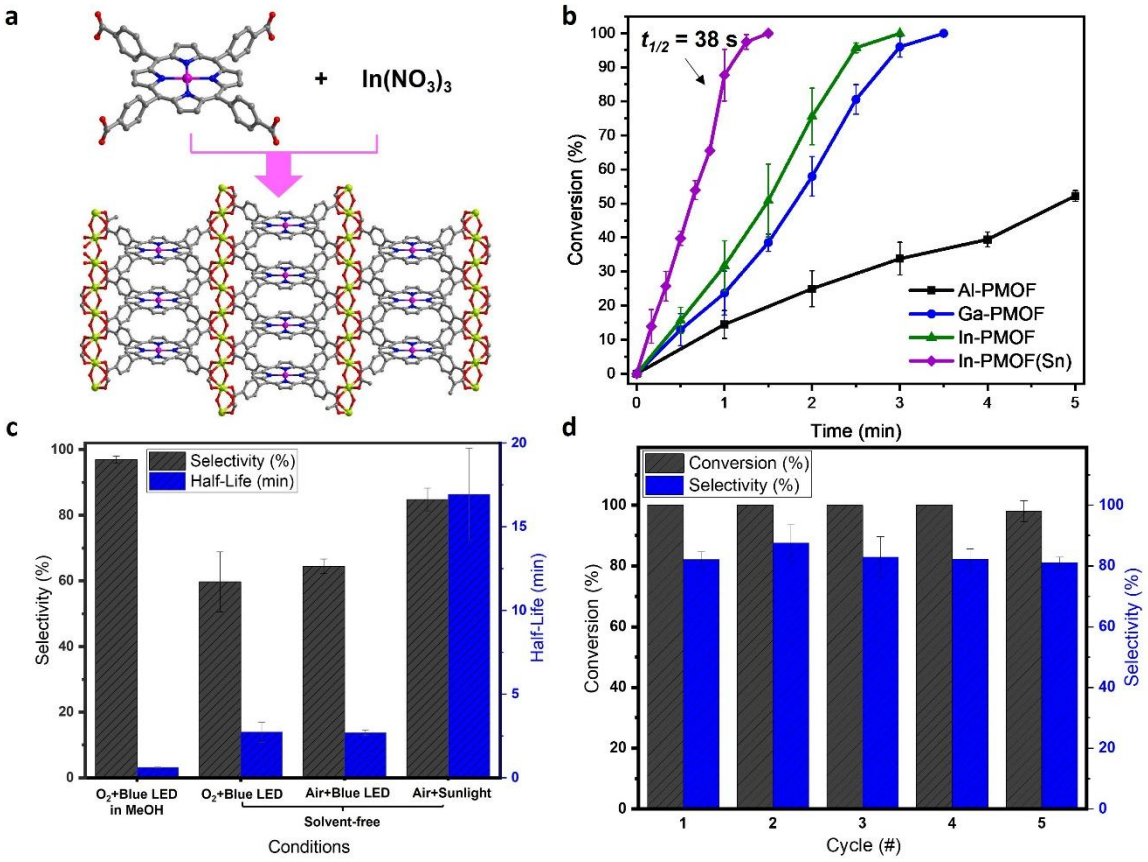

Figure 3. (a) Chemical structure of the Sn-TCPP ligand, the indium precursor salt, and the crystal structure of CSLA-10. (b) Kinetic profile for CEES oxidation in the presence of Al-PMOF, Ga-PMOF, In-PMOF, and CSLA-10 in O_2-saturated methanol under blue LED irradiation. (c) Half-life and selectivity of CEES photooxidation on CSLA-10 textiles containing benzoic acid additives under various conditions. (d) Recyclability test of CSLA-10 textiles containing benzoic acid additives over five consecutive cycles of CEES photooxidation (using air and simulated sunlight).

Sn-TCPP was first synthesized according to previously reported procedures,[19, 36] and successful metalation was confirmed by UV-vis spectroscopy (**Figure S14**). The new MOF, In-

PMOF(Sn) or CSLA-10, was then synthesized via a solvothermal method similar to that used for In-PMOF, with Sn-TCPP replacing the free-base TCPP linker. The structure and phase purity of CSLA-10 were confirmed by PXRD (**Figure S15a**), demonstrating that it is isostructural to the parent In-PMOF. The BET surface area of CSLA-10 was determined from N_2 adsorption measurements at 77 K (**Figure S3d**). CSLA-10 exhibits a lower gravimetric surface area (829 m^2/g) compared to In-PMOF (1,294 m^2/g), attributable to the increased mass resulting from incorporation of Sn^{4+} into the porphyrin linkers. ICP-OES analysis of the digested CSLA-10 revealed a In:Sn molar ratio of 1.32 (**Table S5**), confirming successful incorporation of Sn-TCPP in the framework. SEM images of the CSLA-10 showed sheet-like crystals with particle sizes and morphologies comparable to those of the free base In-PMOF (**Figure S16a**). Energy-dispersive X-ray spectroscopy (EDS) elemental mapping further demonstrated uniform distribution of In and Sn throughout the CSLA-10 crystals (**Figure S17**), providing additional evidence for successful Sn incorporation.

The photocatalytic performance of CSLA-10 toward CEES degradation was first evaluated in MeOH. At a catalyst loading of 0.5 mol% (calculated based on porphyrin centers), complete CEES oxidation was achieved within 1.5 min in the presence of O_2 under blue LED irradiation, corresponding to an exceptionally short CEES half-life of 38 s (**Figure 3b** and **Figure S18**). CSLA-10 exhibits significantly higher activity than the parent In-PMOF ($t_{1/2}$: 38 s vs. 1.4 min), validating our hypothesis that incorporation of a heavy atom into the TCPP ligand enhances photooxidation efficiency. Notably, the combination of heavy In^{3+} nodes and Sn metalation of the porphyrin linker in CSLA-10 produces a synergistic effect, resulting in a greater enhancement of photocatalytic performance than ligand metalation alone (as shown in **Figure S19**).

Notably, a half-life of 38 s represents the shortest reported half-life for CEES degradation among all materials to date (**Table S6**).[19, 24, 37-42] In addition to its remarkable activity, CSLA-10 exhibited high selectivity (97%) toward the nontoxic sulfoxide product in MeOH (**Figure S20**). The types of ROS generated by CSLA-10 were further investigated through trapping and inhibition experiments. These studies confirmed that singlet oxygen is the primary oxidant responsible for CEES photooxidation (**Figures S7**, **S9**, **S23**).

To quantitatively assess the effect of Sn-doping in In-PMOF, we determined the relative singlet oxygen quantum yields of In-PMOF and In-PMOF(Sn) using DMA as a singlet oxygen trap. In deuterated chloroform, nearly all of the singlet oxygen produced by the MOF is trapped by DMA because solvent-mediated deactivation is much slower than reaction with DMA, $k_d << k_r$ [DMA][28] (where k_r is the rate constant of the reaction of singlet oxygen with DMA). Under continuous irradiation and at low conversion of DMA, the amount of singlet oxygen produced remains constant. Plots of the amount of oxidized DMA versus integrated absorbance of the MOF were linear, with slopes proportional to the quantum yield of singlet oxygen production Φ^{Δ}. When irradiation conditions are identical between the two MOFs, the ratio of the slopes directly corresponds to the ratio of the Φ^{Δ} values for the two MOFs. MOF samples with matched integrated absorbances were irradiated at wavelengths above 493 nm in the presence of 50 mM DMA. The resulting plots of the DMA endoperoxide (DMA-O_2) formation versus integrated absorbance yielded a slope ratio of 1.9 for In-PMOF(Sn) to In-MOF (**Figure S24**). These results indicate that Sn doping nearly doubles the singlet oxygen quantum yield of the In-PMOF.

To evaluate the practical applicability of CSLA-10, the MOF was drop-casted onto cotton textiles with benzoic acid additives. The photocatalytic performance of the resulting MOF textile composite was then assessed for CEES degradation under various solvent-free conditions,

including in O_2 with blue LED irradiation, in air with blue LED irradiation, and in air with simulated sunlight irradiation. As shown in **Figure 3c** and **Figure S18**, when using blue LEDs as the light source, the MOF textiles exhibited a half-life of 2.7 min in both O_2 and air, indicating that ambient air provides sufficient O_2 for efficient CEES oxidation. Under these conditions, sulfoxide selectivities of 60% and 64% were observed in O_2 and air, respectively (**Figure S20**). Notably, complete CEES oxidation on the MOF textile was achieved within 7 min in O_2 under blue LEDs, representing the fastest complete CEES degradation reported to date under solvent-free conditions (**Table S2**).[15, 24-27] The CSLA-10 textile was further evaluated in air under simulated sunlight (solar simulator) to assess performance under more practical conditions. A half-life of 16.9 min was observed under these conditions, with a sulfoxide selectivity of 85%, outperforming MOF-525 ($t_{1/2}$ = 17.6 min), a benchmark material reported in our previous study.[15]

A general mechanism for CEES photooxidation is illustrated in **Scheme 1**. Based on our DABCO quenching experiments and established mechanisms for the reaction of singlet oxygen with alkyl sulfides,[15, 43-46] we conclude that singlet oxygen is the sole active oxidant generated by the MOFs. The reaction is initiated by the attack of singlet oxygen on the sulfide, forming a persulfoxide intermediate that is stabilized by hydrogen bonding interactions with MeOH in solution. The persulfoxide intermediate subsequently reacts with a second sulfide molecule to form two sulfoxide products. In protic solvents such as MeOH, where the persulfoxide intermediate is effectively stabilized by hydrogen bond donors, sulfoxides are the primary products. This mechanism is consistent with our observations for CSLA-10, which exhibited a 97% selectivity toward sulfoxide in MeOH (**Figure 3c**). Under solvent-free conditions, however, we observed increased sulfone formation, with sulfoxide selectivity dropping to approximately 60% (**Figure 3c**). This trend is also consistent with the proposed mechanism in **Scheme 1**. Formation of

sulfoxide requires a bimolecular reaction between the persulfoxide intermediate and another sulfide molecule, whereas the collapse of the intermediate to sulfone can proceed via a unimolecular pathway. Under solvent-free conditions, where molecular diffusion is significantly reduced, the bimolecular pathway is less favored, leading to enhanced sulfone formation. Furthermore, the increased sulfoxide selectivity observed in the presence of benzoic acid and air can be attributed to additional hydrogen-bond stabilization of the persulfoxide intermediate, promoted by the benzoic acid and moisture in the air.

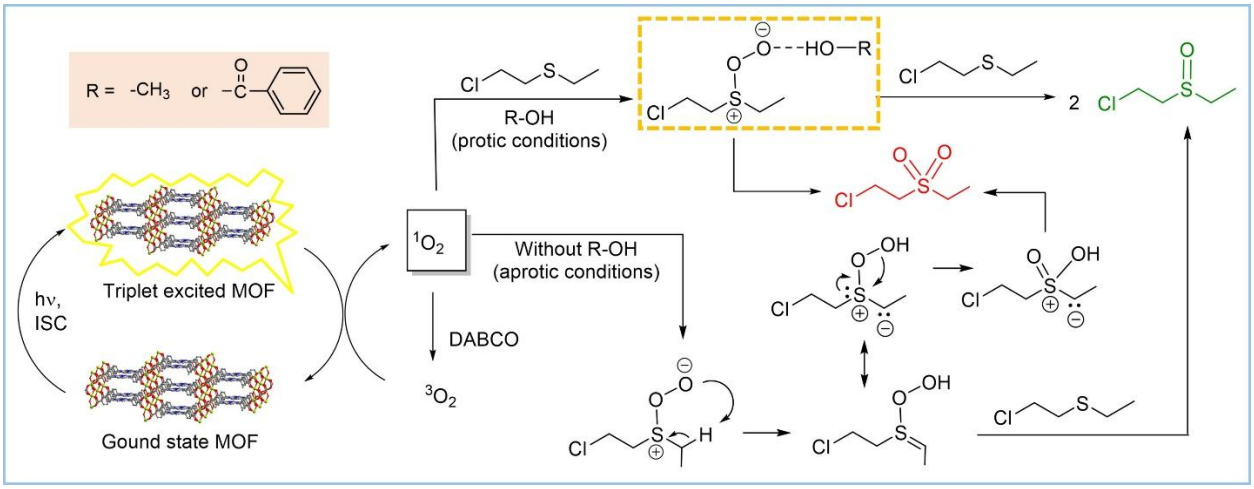

Scheme 1. Proposed mechanism for CEES oxidation by singlet oxygen generated from photoactive MOFs under light irradiation.

Finally, we studied the reusability of the MOF textile for CEES degradation in air under simulated sunlight, representing near-practical conditions. As shown in **Figure 3d**, the MOF textile retained both its catalytic efficiency and selectivity over five consecutive cycles of CEES photooxidation, demonstrating excellent stability and durability. ICP-OES analysis of the recycled CSLA-10 revealed only a slight decrease in the In/Sn ratio, from 1.32 to 1.26, indicating minimal Sn leaching after five catalytic cycles (**Table S5**). In addition, SEM images of the post-catalysis

textiles confirmed the continued presence of MOF particles on the fabric surface after photooxidation (**Figure S16**), underscoring the robustness and reusability of the material.

Conclusions

A series of porphyrin-based MOFs (PMOFs) incorporating different metal nodes (Al, Ga, and In) was synthesized, and their photocatalytic activities toward the degradation of a mustard gas simulant, CEES, were systematically investigated. A clear heavy atom effect was observed among the three isostructural PMOFs (**sea** topology) with comparable surface areas. In-PMOF exhibited the highest activity, achieving a half-life of 1.4 min for CEES degradation, whereas Al-PMOF showed the lowest activity. Motivated by this observation, we rationally designed a new MOF, CSLA-10, featuring indium nodes and Sn-metalated porphyrin linkers. The incorporating of heavy atoms at both the metal nodes and the organic linkers produced synergistic enhancement in photocatalytic performance. In solution, 0.5 mol% CSLA-10 exhibited an exceptionally short CEES half-life of 38 s in MeOH under blue LED irradiation, representing the shortest half-life reported to date. In the solid state, textiles incorporating CSLA-10 achieved complete CEES degradation within 7 min under near-practical conditions. Mechanistic investigations confirmed that singlet oxygen is the primary reactive oxygen species responsible for CEES oxidation. This study provides the first clear demonstration of a heavy atom effect arising from variation of the metal nodes in porphyrin MOFs. By leveraging this design principle, new MOF-based photocatalysts with enhanced photoactivity can be developed for a range of photochemical transformations. Moreover, the excellent performance of CSLS-10 textiles highlights the potential of porphyrin MOFs and their composites for real-world applications in the rapid detoxification of hazardous organic sulfides.

ASSOCIATED CONTENT

Notes

The authors declare no competing financial interest.

Supporting Information.

The Supporting Information is available free of charge at: DOI xx

Instrumentation, Syntheses of MOFs and MOF Composites, Photocatalytic Studies and Stability Tests, Quantum Yield Measurements, Supplementary Figures and Tables (PDF)

ACKNOWLEDGMENT

We acknowledge financial support from the Army Research Office (Grant No. W911NF-19-1-0001). D.M., M.S., and Y.L. also acknowledge the support from NSF PREM (Grant No. DMR 2425229) and NSF CREST (Grant No. HRD-2112554) programs. The photochemical apparatus used for photocatalysis was supported by the U.S. Department of Energy, Office of Science, Office of Basic Energy Sciences, Materials Chemistry Program, under Award No. DE-SC0024498. H.C. acknowledges Southern Methodist University (SMU) for start-up funds and the SMU O'Donnell Data Science and Research Computing Institute for computing resources. Y.L., L.A., and L.Q. were supported by the U.S. Department of Energy (DOE), Office of Basic Energy Sciences, Division of Chemical Sciences, Geosciences, and Biosciences, Catalysis Science program. The Ames National Laboratory is operated for the U.S. DOE by Iowa State University under Contract No. DE-AC02-07CH11358. We wish to thank ISU Chemical Instrumentation Facility staff members Dr. Uddhav Kanbur for training and assistance pertaining to the Elexsys 580 FT-EPR results included in this publication. We also thank Prof. Tian-Fu Liu for her assistance with the topological analysis of all MOFs.

REFERENCES

1. Luo, L.; Zhang, T.; Wang, M.; Yun, R.; Xiang, X., Recent Advances in Heterogeneous Photo-Driven Oxidation of Organic Molecules by Reactive Oxygen Species. *ChemSusChem* **2020,** *13* (19), 5173-5184.
2. Wen, Y.; Feng, M.; Zhang, P.; Zhou, H.-C.; Sharma, V. K.; Ma, X., Metal Organic Frameworks (MOFs) as Photocatalysts for the Degradation of Agricultural Pollutants in Water. *ACS ES&T Eng.* **2021,** *1* (5), 804-826.
3. Fernández-Castro, P.; Vallejo, M.; San Román, M. F.; Ortiz, I., Insight on the fundamentals of advanced oxidation processes. Role and review of the determination methods of reactive oxygen species. *J. Chem. Technol. Biotechnol.* **2015,** *90* (5), 796-820.
4. Zhang, Y.; Pang, J.; Li, J.; Yang, X.; Feng, M.; Cai, P.; Zhou, H.-C., Visible-light harvesting pyrene-based MOFs as efficient ROS generators. *Chem. Sci.* **2019,** *10* (36), 8455-8460.
5. Liu, Y.; Howarth, A. J.; Vermeulen, N. A.; Moon, S.-Y.; Hupp, J. T.; Farha, O. K., Catalytic degradation of chemical warfare agents and their simulants by metal-organic frameworks. *Coord. Chem. Rev.* **2017,** *346*, 101-111.
6. Guo, Z.; Liu, X.; Bai, R.; Che, Y.; Chi, Y.; Guo, C.; Xing, H., Photoactive Metal–Organic Frameworks for the Selective Synthesis of Thioethers: Coupled with Phosphine to Modulate Thiyl Radical Generation. *Inorg. Chem.* **2021,** *60* (12), 8672-8681.
7. Wang, X.; Dong, M.-J.; Wu, C.-D., Tuning the pore structures and photocatalytic properties of a 2D covalent organic framework with multi-branched photoactive moieties. *Nanoscale* **2020,** *12* (30), 16136-16142.
8. Wang, C.-C.; Li, J.-R.; Lv, X.-L.; Zhang, Y.-Q.; Guo, G., Photocatalytic organic pollutants degradation in metal–organic frameworks. *Energy Environ. Sci.* **2014,** *7* (9), 2831-2867.

9. Wang, S.; Sun, Q.; Chen, W.; Tang, Y.; Aguila, B.; Pan, Y.; Zheng, A.; Yang, Z.; Wojtas, L.; Ma, S.; Xiao, F.-S., Programming Covalent Organic Frameworks for Photocatalysis: Investigation of Chemical and Structural Variations. *Matter* **2020,** *2* (2), 416-427.

10. Ni, K.; Lan, G.; Lin, W., Nanoscale Metal–Organic Frameworks Generate Reactive Oxygen Species for Cancer Therapy. *ACS Cent. Sci.* **2020,** *6* (6), 861-868.

11. Zhang, X.; Wasson, M. C.; Shayan, M.; Berdichevsky, E. K.; Ricardo-Noordberg, J.; Singh, Z.; Papazyan, E. K.; Castro, A. J.; Marino, P.; Ajoyan, Z.; Chen, Z.; Islamoglu, T.; Howarth, A. J.; Liu, Y.; Majewski, M. B.; Katz, M. J.; Mondloch, J. E.; Farha, O. K., A historical perspective on porphyrin-based metal–organic frameworks and their applications. *Coord. Chem. Rev.* **2021,** *429*, 213615.

12. Chen, J.; Zhu, Y.; Kaskel, S., Porphyrin-Based Metal–Organic Frameworks for Biomedical Applications. *Angew. Chem. Int. Ed.* **2021,** *60* (10), 5010-5035.

13. Liu, F.; Rincón, I.; Baldoví, H. G.; Dhakshinamoorthy, A.; Horcajada, P.; Rojas, S.; Navalón, S.; Fateeva, A., Porphyrin-based MOFs for photocatalysis in water: advancements in solar fuels generation and pollutants degradation. *Inorg. Chem. Front.* **2024,** *11* (8), 2212-2245.

14. Liu, Y.; Howarth, A. J.; Hupp, J. T.; Farha, O. K., Selective Photooxidation of a Mustard-Gas Simulant Catalyzed by a Porphyrinic Metal-Organic Framework. *Angewandte Chemie (International ed. in English)* **2015,** *54* (31), 9001-5.

15. Hao, Y.; Papazyan, E. K.; Ba, Y.; Liu, Y., Mechanism-Guided Design of Metal–Organic Framework Composites for Selective Photooxidation of a Mustard Gas Simulant under Solvent-Free Conditions. *ACS Catal.* **2022,** *12* (1), 363-371.

16. Darmanyan, A. P.; Foote, C. S., Effect of sensitizer heavy atoms on singlet oxygen generation efficiency. *J. Phys. Chem.* **1992,** *96* (9), 3723-3728.

17. Azenha, E. l. G.; Serra, A. C.; Pineiro, M.; Pereira, M. M.; Seixas de Melo, J.; Arnaut, L. G.; Formosinho, S. J.; Rocha Gonsalves, A. M. d. A., Heavy-atom effects on metalloporphyrins and polyhalogenated porphyrins. *Chem. Phys.* **2002,** *280* (1), 177-190.

18. Harriman, A., Luminescence of porphyrins and metalloporphyrins. Part 3.—Heavy-atom effects. *J. Chem. Soc., Faraday Trans. 2* **1981,** *77* (7), 1281-1291.

19. Quon, A. S.; Manriquez, D.; Nguyen, A.; Papazyan, E. K.; Wijeratne, P.; An, L.; Qi, L.; Tang, M. J.; Ready, A. D.; Farha, O. K.; Liu, Y., Metalloporphyrinic metal–organic frameworks for enhanced photocatalytic degradation of a mustard gas simulant. *Chem. Commun.* **2025,** *61* (1), 77-80.

20. Quezada-Novoa, V.; Titi, H. M.; Sarjeant, A. A.; Howarth, A. J., Building a shp: A Rare-Earth Metal–Organic Framework and Its Application in a Catalytic Photooxidation Reaction. *Chem. Mater.* **2021,** *33* (11), 4163-4169.

21. Quezada-Novoa, V.; Titi, H. M.; Villanueva, F. Y.; Wilson, M. W. B.; Howarth, A. J., The Effect of Linker-to-Metal Energy Transfer on the Photooxidation Performance of an Isostructural Series of Pyrene-Based Rare-Earth Metal–Organic Frameworks. *Small* **2023,** *19* (36), 2302173.

22. Fateeva, A.; Chater, P. A.; Ireland, C. P.; Tahir, A. A.; Khimyak, Y. Z.; Wiper, P. V.; Darwent, J. R.; Rosseinsky, M. J., A Water-Stable Porphyrin-Based Metal–Organic Framework Active for Visible-Light Photocatalysis. *Angew. Chem. Int. Ed.* **2012,** *51* (30), 7440-7444.

23. Rhauderwiek, T.; Waitschat, S.; Wuttke, S.; Reinsch, H.; Bein, T.; Stock, N., Nanoscale Synthesis of Two Porphyrin-Based MOFs with Gallium and Indium. *Inorg. Chem.* **2016,** *55* (11), 5312-5319.

24. Wu, M.-M.; Su, J.; Luo, D.; Cai, B.-C.; Zheng, Z.-L.; Bin, D.-S.; Li, Y. Y.; Zhou, X.-P., Ultrafast Photocatalytic Detoxification of Mustard Gas Simulants by a Mesoporous Metal–Organic Framework with Dangling Porphyrin Molecules. *Small* **2023,** *19* (36), 2301050.

25. Lee, D. T.; Jamir, J. D.; Peterson, G. W.; Parsons, G. N., Protective Fabrics: Metal-Organic Framework Textiles for Rapid Photocatalytic Sulfur Mustard Simulant Detoxification. *Matter* **2020,** *2* (2), 404-415.

26. Ma, K.; Li, P.; Xin, J. H.; Chen, Y.; Chen, Z.; Goswami, S.; Liu, X.; Kato, S.; Chen, H.; Zhang, X.; Bai, J.; Wasson, M. C.; Maldonado, R. R.; Snurr, R. Q.; Farha, O. K., Ultrastable Mesoporous Hydrogen-Bonded Organic Framework-Based Fiber Composites toward Mustard Gas Detoxification. *Cell Rep. Phys. Sci.* **2020,** *1* (2), 100024.

27. Barton, H. F.; Jamir, J. D.; Davis, A. K.; Peterson, G. W.; Parsons, G. N., Doubly Protective MOF-Photo-Fabrics: Facile Template-Free Synthesis of PCN-222-Textiles Enables Rapid Hydrolysis, Photo-Hydrolysis and Selective Oxidation of Multiple Chemical Warfare Agents and Simulants. *Chem. Eur. J.* **2021,** *27* (4), 1465-1472.

28. Hao, Y.; Liu, B. M.; Bennett, T. F.; Monsour, C. G.; Selke, M.; Liu, Y., Determination of Singlet Oxygen Quantum Yield of a Porphyrinic Metal–Organic Framework. *J. Phys. Chem. C.* **2021,** *125* (13), 7392-7400.

29. Yin, J.; Huang, C.; Zhou, Y.; Zhang, L.; Li, N.; Sun, R., Selective Oxidation of 2-Chloroethyl Ethyl Sulfide in Aqueous Media Catalyzed by {Mo72M30} Nano-polyoxometalate Clusters Differentiating the Catalytic Activity of Nodal Metals. *Ind. Eng. Chem. Res.* **2022,** *61* (23), 7699-7708.

30. Buru, C. T.; Wasson, M. C.; Farha, O. K., H5PV2Mo10O40 Polyoxometalate Encapsulated in NU-1000 Metal–Organic Framework for Aerobic Oxidation of a Mustard Gas Simulant. *ACS Appl. Nano Mater.* **2020,** *3* (1), 658-664.

31. Foote, C., *Chemical mechanisms of photodynamic action*. SPIE: 1990; Vol. 10306.

32. Foote, C. S.; Peterson, E. R.; Lee, K.-W., Chemistry of singlet oxygen. XVI. Long lifetime of singlet oxygen in carbon disulfide. *J. Am. Chem. Soc.* **1972,** *94* (3), 1032-1033.

33. Kacher, M. L.; Foote, C. S., Chemistry of Singlet Oxygen—XXVIII. Steric and Electronic Effects on the Reactivity of Sulfides with Singlet Oxygen. *Photochem. Photobiol.* **1979,** *29* (4), 765-769.

34. Silverman, S. K.; Foote, C. S., Singlet oxygen and electron-transfer mechanisms in the dicyanoanthracene-sensitized photooxidation of 2,3-diphenyl-1,4-dioxene. *J. Am. Chem. Soc.* **1991,** *113* (20), 7672-7675.

35. Bonesi, S. M.; Albini, A., Effect of Protic Cosolvents on the Photooxygenation of Diethyl Sulfide. *J. Org. Chem.* **2000,** *65* (15), 4532-4536.

36. Manke, A.-M.; Geisel, K.; Fetzer, A.; Kurz, P., A water-soluble tin(iv) porphyrin as a bioinspired photosensitiser for light-driven proton-reduction. *Phys. Chem. Chem. Phys.* **2014,** *16* (24), 12029-12042.

37. Gong, C.-H.; Sun, Z.-B.; Cao, M.; Luo, X.-M.; Wu, J.; Wang, Q.-Y.; Zang, S.-Q.; Mak, T. C. W., Phosphate anion-induced silver-chalcogenide cluster-based metal organic frameworks as dual-functional catalysts for detoxifying chemical warfare agent simulants. *Chem. Commun.* **2022,** *58* (70), 9806-9809.

38. Zhao, H.; Tao, C.-a.; Zhao, S.; Zou, X.; Wang, F.; Wang, J., Porphyrin-Moiety-Functionalized Metal–Organic Layers Exhibiting Catalytic Capabilities for Detoxifying Nerve Agent and Blister Agent Simulants. *ACS Appl. Mater. Interfaces* **2023,** *15* (2), 3297-3306.

39. Zhou, J.; Li, X.; Chu, C.; Cao, J., One-pot synthesis of a porphyrin functionalized metal-organic frameworks as a recyclable visible-light-driven photosensitizer for efficient detoxification of a sulfur mustard simulant in air. *Microporous and Mesoporous Mater.* **2024,** *375*, 113163.

40. Cao, M.; Pang, R.; Wang, Q.-Y.; Han, Z.; Wang, Z.-Y.; Dong, X.-Y.; Li, S.-F.; Zang, S.-Q.; Mak, T. C. W., Porphyrinic Silver Cluster Assembled Material for Simultaneous Capture and Photocatalysis of Mustard-Gas Simulant. *J. Am. Chem. Soc.* **2019,** *141* (37), 14505-14509.

41. Wu, W.; He, T.; Zhang, X.; Xie, L.-H.; Si, G.-R.; Xie, Y.; Li, J.-R., Rare-Earth Metal–Organic Framework with Nonplanar Porphyrin Groups for High-Efficiency Photocatalysis. *Inorg. Chem.* **2024,** *63* (16), 7412-7421.

42. Lee, M. S.; Garibay, S. J.; Ploskonka, A. M.; DeCoste, J. B., Bioderived protoporphyrin IX incorporation into a metal-organic framework for enhanced photocatalytic degradation of chemical warfare agents. *MRS Commun.* **2019,** *9* (2), 464-473.

43. Jensen, F.; Greer, A.; Clennan, E. L., Reaction of Organic Sulfides with Singlet Oxygen. A Revised Mechanism. *J. Am. Chem. Soc.* **1998,** *120* (18), 4439-4449.

44. Toutchkine, A.; Clennan, E. L., The reactions of singlet oxygen with β-chlorosulfides. The role of hydroperoxy sulfonium ylides in the oxidative destruction of chemical warfare simulants. *Tetrahedron Lett.* **1999,** *40* (36), 6519-6522.

45. Liu, Y.; Buru, C. T.; Howarth, A. J.; Mahle, J. J.; Buchanan, J. H.; DeCoste, J. B.; Hupp, J. T.; Farha, O. K., Efficient and selective oxidation of sulfur mustard using singlet oxygen generated by a pyrene-based metal–organic framework. *J. Mater. Chem. A* **2016,** *4* (36), 13809-13813.

46. Liang, J. J.; Gu, C. L.; Kacher, M. L.; Foote, C. S., Chemistry of singlet oxygen. 45. Mechanism of the photooxidation of sulfides. *J. Am. Chem. Soc.* **1983,** *105* (14), 4717-4721.

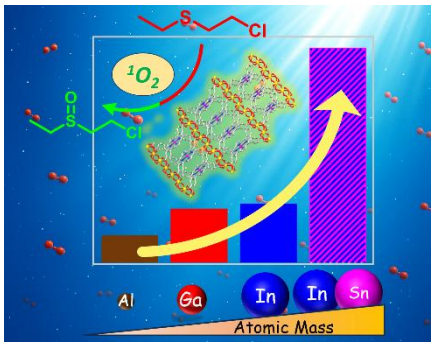

A heavy atom effect was observed in a series of porphyrin-based metal–organic frameworks (PMOFs) with a sea topology. Building on this finding, we synthesized a novel MOF incorporating indium nodes and tin-doped porphyrin linkers, which exhibited high efficiency in both solution- and solid-phase photooxidation of a mustard gas simulant.